

SIMULATION OF BOUNDARY STATES OF HELICOPTER FLIGHT

Jarosław Stanisławski

Lukasiewicz Research Network – Institute of Aviation
Krakowska Av. 110/114, 02-256 Warsaw, Poland
tel.: +48 22 8460011 ext. 362
e-mail: jaroslaw.stanislawski@ilot.edu.pl

Abstract

Results of simulation of main rotor blade loads and deformations, which can be generated during boundary states of helicopter flight, are presented. Concerned cases of flight envelope include hover at maximum height, level flight at high velocity, pull-up manoeuvres applying cyclic pitch and mixed collective and cyclic control. The simulation calculations were executed for data of light helicopter with three-bladed articulated rotor. For analysis, the real blades are treated as elastic axes with distributed masses of blade segments. The model of deformable blade allows for out-of-plane bending, in plane bending, and torsion. For assumed flight state of helicopter, the equations of rotor blades motion are solved applying Runge-Kutta method. According to Galerkin method, for each concerned azimuthal position of blade the parameters of its motions are assumed as a combination of considered bending and torsion eigen modes of the blade. The loads of rotor blades generated during flight depend due to velocity of flight, helicopter mass, position of rotor axis in air and deflections of swashplate that correspond to collective and cyclic pitch angle applied to rotor blades. The results of simulations presenting rotor loads and blade deformations are shown in form of time-runs and as plots of rotor-disk distributions. The simulations of helicopter flight states may be useful for prediction the conditions of flight-tests without exceeding safety boundaries or may help to define limitations for manoeuvre and control of helicopter.

Keywords: helicopter, boundary flight, rotor loads

1. Introduction

The problems of helicopter designing and development are in large range related to high level of loads and vibration generated on rotor blades. For helicopter flight conditions, besides hover, the components of blade cross-section airflows are changed from low velocity for retreating blade position to high speed for advancing blade. The collective and cyclic control of the blade pitch introduces additional dynamic loads, which affect variable deflections of rotor blades. To predict the level of rotor loads, which can be generated in different states of flight, the codes of computer programs were developed which enable analysis of rotor behaviour in typical helicopter operation and at boundaries of flight envelope [2, 6, 7]. Among applied codes the following could be mentioned: CAMRAD (Comprehensive Analytical Model of Rotorcraft Aerodynamics and Dynamics) developed for NASA and US Army, FLIGHTLAB developed in USA by Advanced Rotorcraft Technology, Inc., DYMORE developed at the Georgia Institute of Technology and German-French HOST (Helicopter Overall Simulation Tool) developed by DLR and ONERA. Flight test measurements [3, 4] and wind tunnel investigations [10] provide data for verification the analytical methods applied for defining loads of helicopter rotor. Introduction CFD/CSD methods [1, 9] which couple computational fluid dynamics and analysis of flexible body dynamics allows to improve the accuracy of prediction the rotor blades loads.

In the Institute of Aviation, during designing the ILX-27 unmanned helicopter [5] a home-developed simulation program for rotor loads calculation was applied. Presented in the paper results of simulation the loads of rotor blades were calculated for data of the three-bladed rotor of the hypothetical light helicopter with take-off mass equal 1,100 kg. Designed in the Institute of Aviation airfoils of ILH family [8] were applied for blades of the main rotor. In the case of

considered flight states including hover, flight at high speed and pull-up manoeuvres, the simulations are carried out for quasi-steady conditions with constant rotor speed, constant pitch of rotor shaft and constant blade collective and cyclic control due to swashplate position. The comparisons of calculated rotor loads and blade deflections are shown in the time-plots or rotor disk distributions for the cases of helicopter flight envelope.

2. Model of helicopter rotor

The model of helicopter rotor consists of the elastic axes with sets of lumped masses of blade segments distributed along each blade of rotor. The scheme of rotor blade model is shown in Fig. 1. The elastic axis is assumed to allow blade torsion and bending in plane and out-of-plane. In accordance with Galerkin method, blade deformations and parameters of blade motion are considered as combinations of applied torsion and bending eigen modes. The deflections of the blade elastic axis y, z, φ are treated as superposition of modal components:

$$y(x,t) = \sum_{i=1}^I \rho_i(t) y_i(x), \quad z(x,t) = \sum_{j=1}^J \delta_j(t) z_j(x), \quad \varphi(x,t) = \sum_{k=1}^K \eta_k(t) \varphi_k(x), \quad (1)$$

where:

y_i, z_j, φ_k – eigen modes of in plane, out-of-plane bending and torsion respectively,

ρ_i, δ_j, η_k – time dependent shares of eigen modes determined in computing process,

I, J, K – numbers of applied bending and torsion eigen modes.

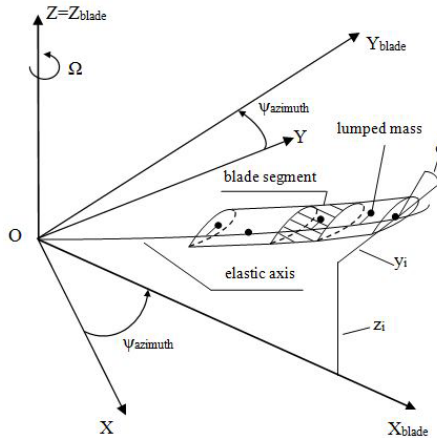


Fig. 1. Scheme of rotor blade model with lumped masses and elastic axis

To define quasi-steady conditions necessary for simulation the chosen state of flight the simplified model of helicopter is applied. This auxiliary model consists of fuselage reduced to point mass with assigned aerodynamic characteristics and main rotor treated as disk area with averaged value of induced velocity and aerodynamic coefficients. The simplified model of helicopter provides data demanded for helicopter equilibrium: pitch of rotor shaft, components of rotor thrust, initial position of swashplate.

The equations of motion of elastic blades are solved applying the Runge-Kutta method. Blade deflections variable with azimuthal position on rotor disk mutually affect aerodynamic and inertial forces, which are generated at blade sections. Aerodynamic forces acting on segment of blade at given azimuth position are computed applying the blade element theory. The cycle of calculations repeated for changed with step $\Delta\psi$ blade azimuthal position provides data for defining the distributions of blade deformations and loads on rotor disk. The aerodynamic forces and local angle of attack at blade cross-section depend on pitch angle control and temporary components of airflow:

$$\alpha = \varphi_o + \varphi_x \cos \Omega t + \varphi_y \sin \Omega t + \varphi_{geom} + \Delta\varphi_{torsion} - \text{arc tg} \left(\frac{u_z}{u_x} \right), \quad (2)$$

where:

- φ_o – blade collective control angle,
- φ_x, φ_y – cyclic control angle due to roll and pitch deflections of the swashplate,
- φ_{geom} – blade geometric twist,
- $\Delta\varphi_{torsion}$ – local torsion deformation,
- u_z, u_x – components of the cross-section airflow of rotor blade: out-of-plane and in plane.

3. Results of simulation

Results of calculation concerning power required for flight and equilibrium conditions due to speed of helicopter are shown in Fig. 2. Helicopter performances depend on relation mass of helicopter to available power of engine. In hover increased take-off mass or higher flight altitude demand enlarged power of engine. Transition from hover to level flight is accompanied by reduction the value of total power required to flight until to speed of economical conditions close to speed of 100 km/h.

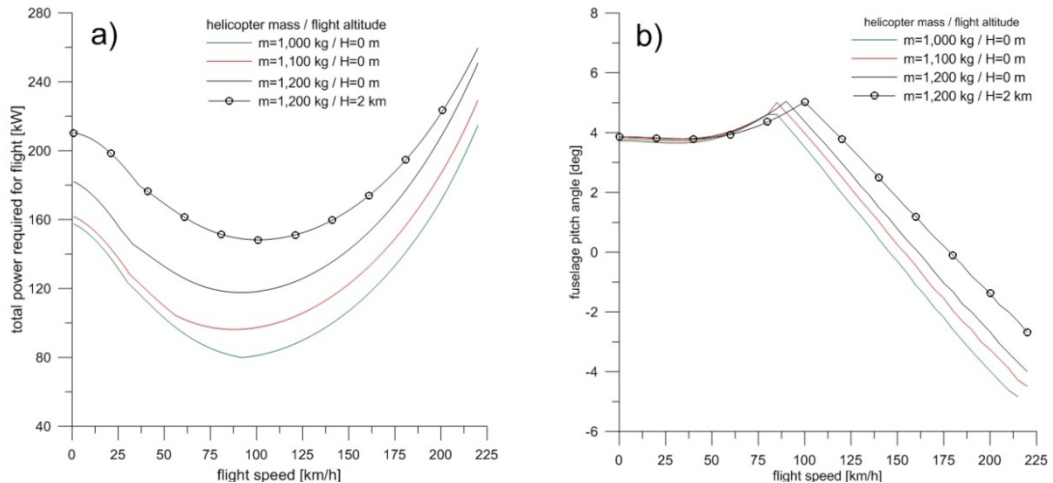


Fig. 2. Comparison due to flight speed: a) total power required for flight, b) fuselage pitch in equilibrium conditions

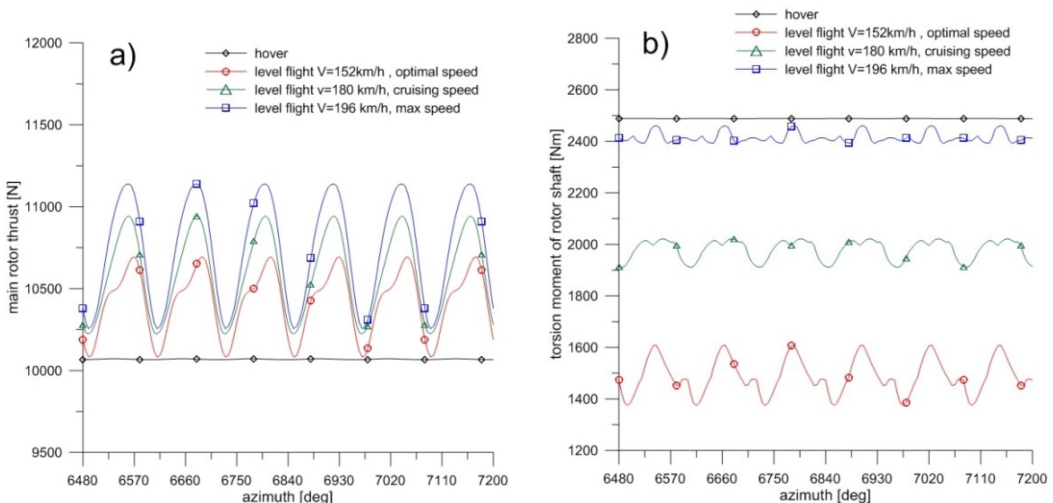


Fig. 3. Comparison of time-runs: a) main rotor thrust, b) torsion moment of rotor shaft for hover and level flight conditions

Further increase of flight speed to maximum velocity can be accomplished with higher level of power required. The aerodynamic drag of fuselage is overcome by horizontal component of rotor thrust which is generated by swashplate deflection and pitching the fuselage of helicopter.

The calculations of rotor load components and blade deformations were performed for time equals to 20 revolutions of the main rotor and with change step of blade azimuthal position $\Delta\psi$ equal 5° . The presented time-plots for the calculation cases (Fig. 3-9) are related to the last two rotor revolutions of simulation. Comparison of main rotor thrust and torsion moment of rotor shaft from hover to conditions of maximum level speed for helicopter with mass of 1,100 kg are presented in Fig. 3. For increased flight speed, the higher value of rotor thrust is observed.

Arising amplitude of thrust is associated with growing, due to higher speed, the differences of airflow conditions between position of advancing blade at azimuth 90° and retreating blade at azimuth 270° on rotor disk. The time-run of thrust includes three cycles per one revolution, which is characteristic for three-bladed rotor. The value of rotor shaft torsion moment is related with level of power required for flight. Similar high torsion moments are noticed for hover and flight with maximum speed (Fig. 3b) The blade control moments increasing with flight speed indicate growth of rotor blade loads (Fig. 4a).

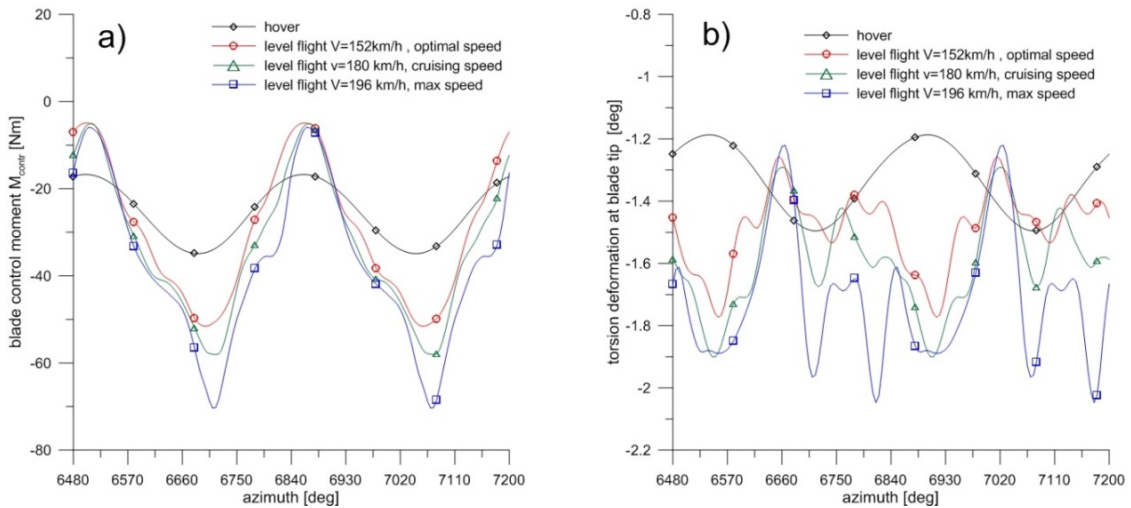


Fig. 4. Comparison of time-runs: a) blade control moment, b) blade torsion deformation at tip for hover and level flight conditions

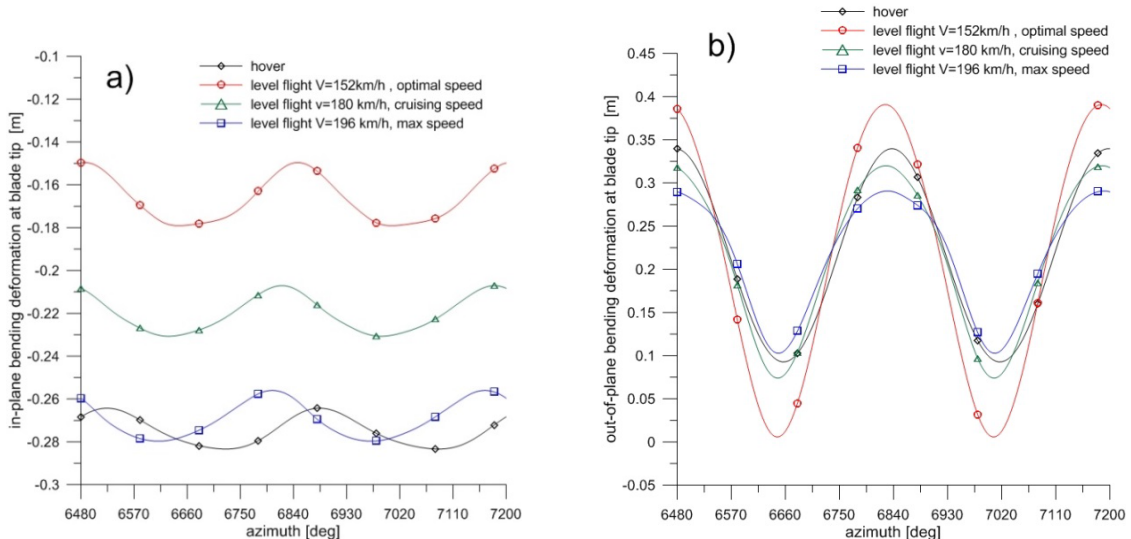


Fig. 5. Comparison of bending deflection at blade tip for hover and level flight conditions:
a) in-plane bending deformation, b) out-of-plane bending deformation

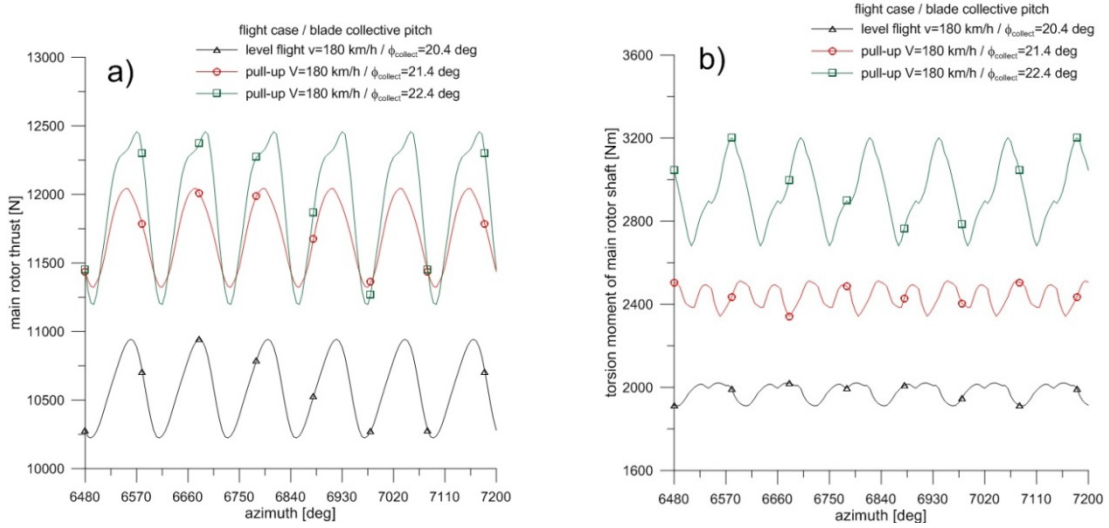


Fig. 6. Time-plots: a) main rotor thrust, b) torsion moment of rotor shaft in collective pull-up at speed of 180 km/h, mass of helicopter $m = 1,100 \text{ kg}$, constant pitch of rotor shaft axis, constant swashplate pitch

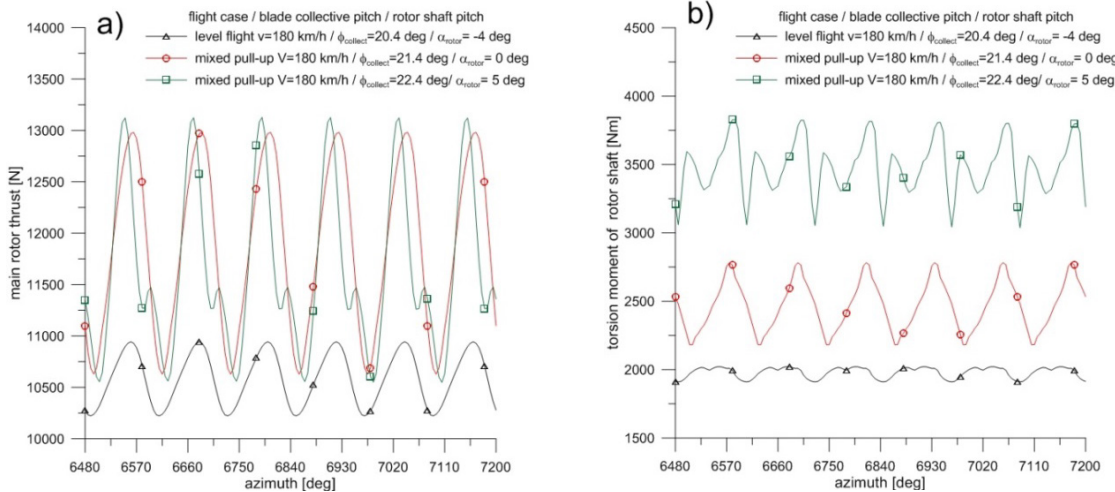


Fig. 7. Time-plots: a) main rotor thrust, b) torsion moment of rotor shaft in mixed pull-up at speed of 180 km/h, mass of helicopter $m = 1,100 \text{ kg}$

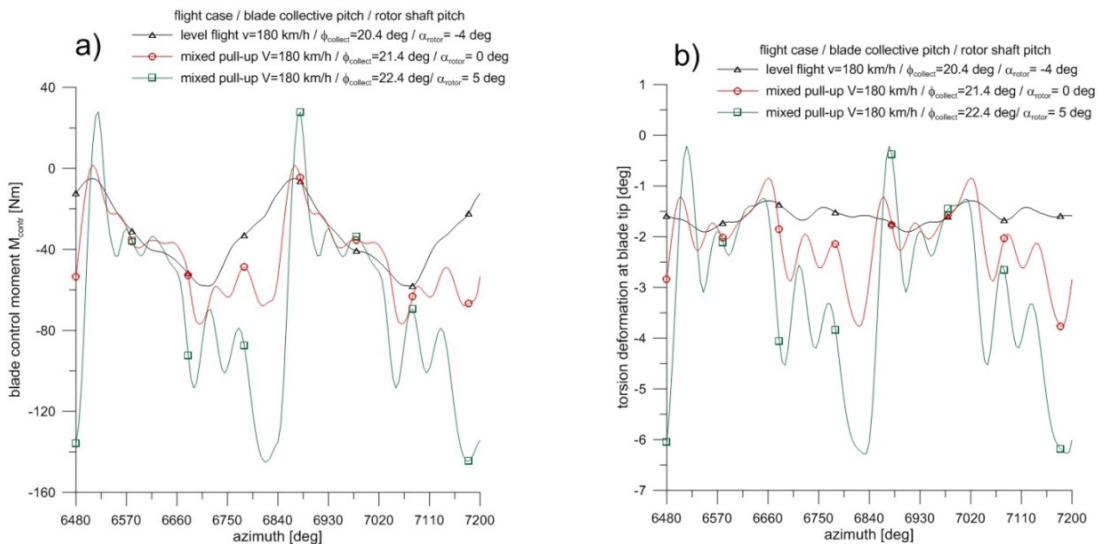


Fig. 8. Time-plots: a) blade control moment, b) torsion deformation at blade tip in mixed pull-up at speed of 180 km/h, mass of helicopter $m = 1,100 \text{ kg}$

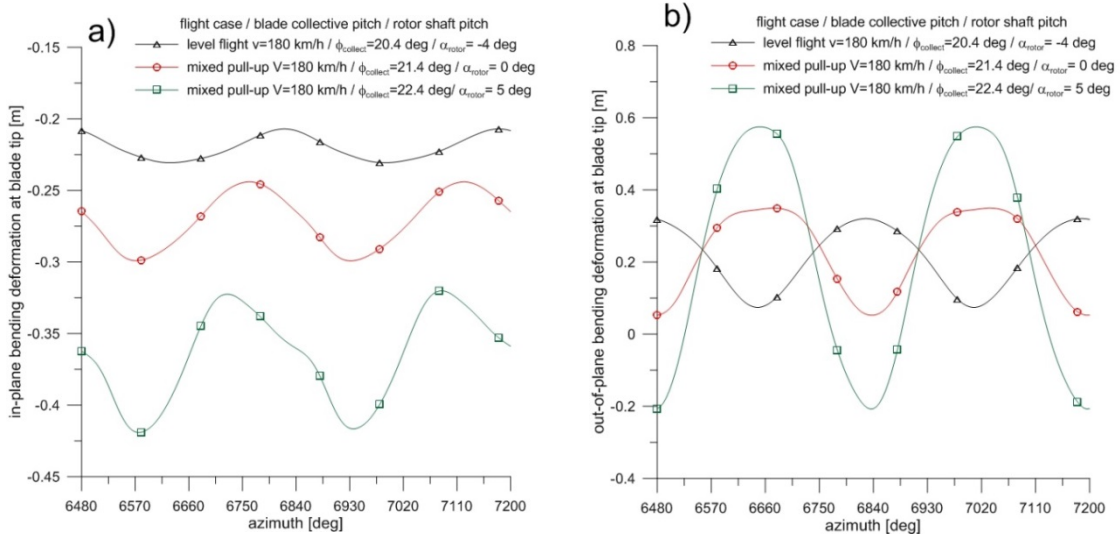


Fig. 9. Time-plots of blade bending deformations in mixed pull-up at speed of 180 km/h, mass of helicopter $m = 1,100 \text{ kg}$: a) in-plane bending deformation at blade tip, b) out-of-plane bending deformation at blade tip

The blade control moments during rotor revolution are influenced by variable airflow, blade cyclic and collective pitch control due to swashplate deflections and mutual blade torsion deformations (Fig. 4b). Variable aerodynamic and inertial forces acting on blade segment generate torsion deformations as well in-plane bending (Fig. 5a) and out-of-plane bending (Fig. 5b) of rotor blades. Variable blade deformations for the hover are connected with data of the calculation case for which the position of helicopter centre. Mass is shifted relative to the rotor shaft axis, so to reach equilibrium condition, the swashplate should be deflected. In Fig. 6 and Fig. 7 are shown time-plots of rotor thrust and torsion moments of rotor shaft for the initial phase of collective pull-up manoeuvre without change of fuselage pitch and mixed pull-up manoeuvre with changed fuselage pitch angle and changed cyclic and collective blade control pitch.

Comparison of the two methods of realization the pull-up manoeuvres indicates that in mixed pull-up the higher thrust can be developed but also with the higher amplitude generated during rotor revolution (Fig. 6a, Fig. 7a). In the mixed pull-up, the higher amplitudes can be noticed for rotor shaft torsion moments (Fig. 6b, Fig. 7b). With tilted up nose of fuselage in the case of mixed pull-up the enlarged component of air flows from bottom surface of rotor disk to upper one which, besides the collective blade pitch, influences increase the local attack angles of blades and results in sharp growth of blade loads, including blade control moments (Fig. 8a). The increased rotor loads generate higher level of blade torsion deformations (Fig. 8b) and blade bending deformations (Fig. 9a, b). In Fig. 8 and Fig. 9 are shown blade deformations at tip section. The rotor disk distributions of local attack angles and differences of critical and attack angles for collective pull-up (Fig. 10) and mixed pull-up (Fig. 11) allow for better view at different airflow conditions.

In the case of collective pull-up, the maximum attack angles reach value of 12-13° for retreating blade positions close to azimuth of 270° (Fig. 10a). The narrow zone of separated flow is limited to blade tip, which is signed by thick izoline of zero value in Fig. 10b. In the rotor disk distribution of attack angles for mixed pull-up the large area of attack angles reaching values of 18-20° can be noticed in vicinity of retreating blade position (Fig. 11a). Increase of attack angles observed at left side of rotor disk results in generation the vast zone of separated flow whose borders are indicated by izoline 0 in Fig. 11b. Effects of blade passage through the borders of separated airflow zone can be noticed in rotor disk distributions of blade torsion deformations (Fig. 12). In the case of mixed pull-up (Fig. 12b) enlarged torsion oscillations of blade are caused by sudden changes of aerodynamic loads during crossing the borders of separated flow. Decrease of blade pitch control rate in manoeuvre or beginning the sharp manoeuvre at lower flight speed may diminish excessive growth of rotor loads.

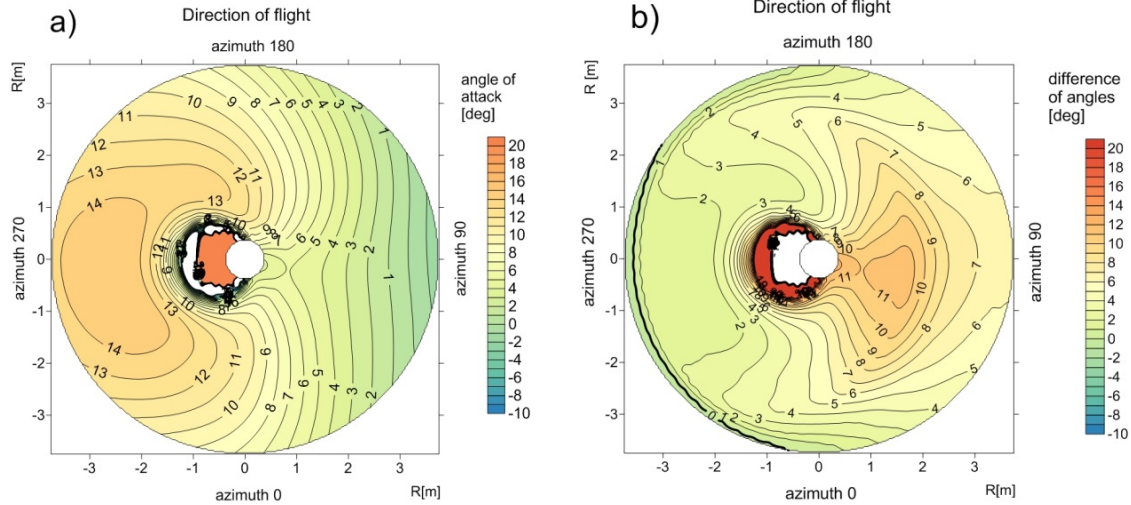


Fig. 10. Rotor disk distributions in collective pull-up at speed of 180 km/h for rotor shaft axis pitch -3.96 deg and blade collective pitch 21.44 deg: a) local attack angle, b) difference of critical and local attack angles of blade cross-sections

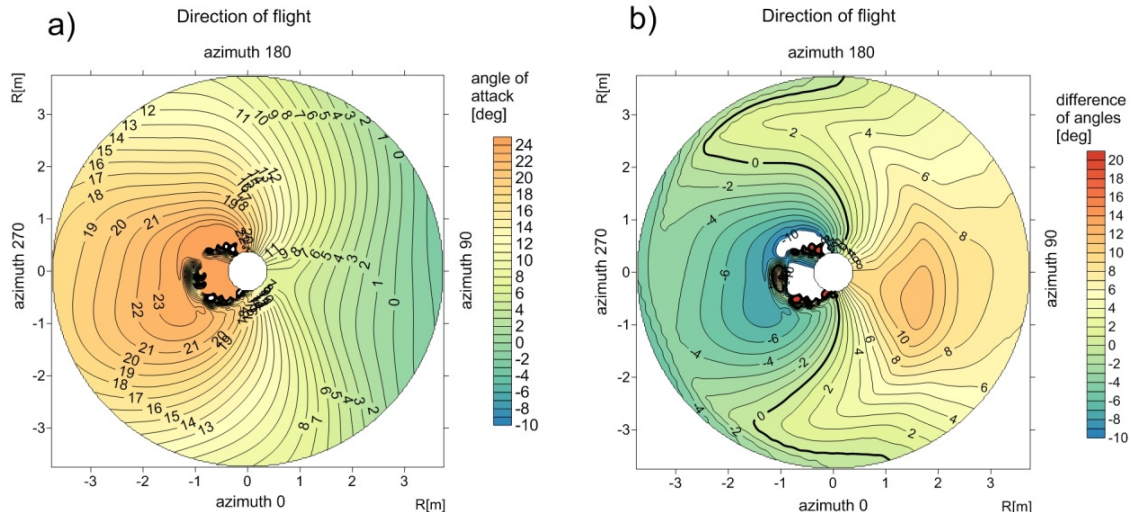


Fig. 11. Rotor disk distributions in mixed pull-up at speed of 180 km/h for rotor shaft axis pitch 0.0 deg and blade collective pitch 21.44 deg: a) local attack angle, b) difference of critical and local attack angles

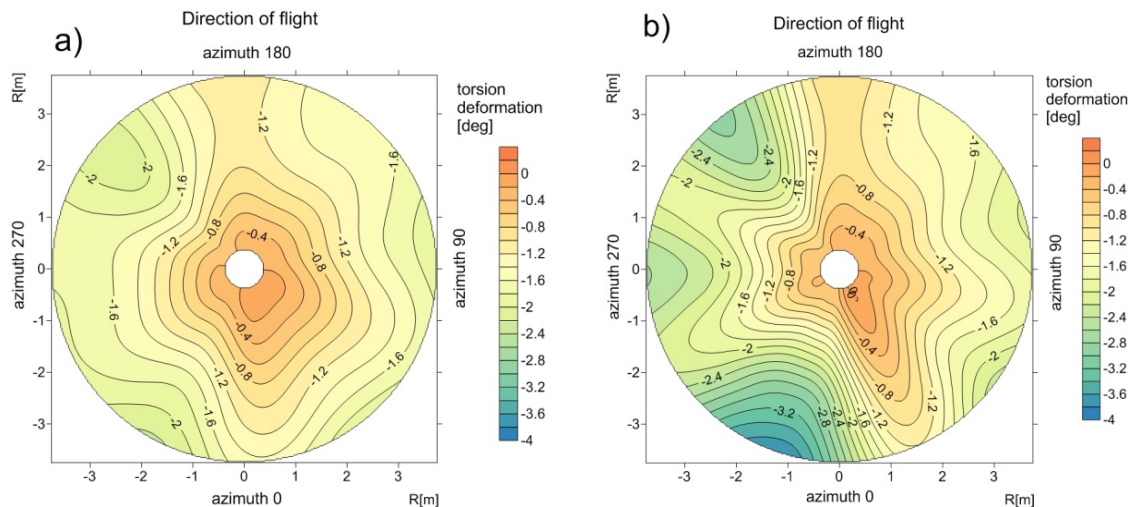


Fig. 12. Rotor disk distributions of blade torsion deformation at speed of 180 km/h
a) in collective pull-up, b) in mixed pull-up

4. Conclusions

The simulation program for calculation helicopter performance, rotor loads and blade deformations can be applied in early phase of design a new rotorcraft or for prediction the results of modifications of helicopter characteristics. Analysis of rotor loads and blades behaviour in different helicopter flight states may be useful for defining the limits for helicopter control and execution of manoeuvres.

References

- [1] Bain, J., Sim, B. W., Sankar, L., Brentner, K., *Aeromechanics and Aeroacoustics Predictions of the Boeing -SMART Rotor Using Coupled -CFD/CSD Analysis*, AHS 66th Annual Forum, Phonix, Arizona 2010.
- [2] Bousman, W. G., *Putting the Aero Back Into Aeroelasticity*, NASA/TM-2000-209589, Ames Research Center Moffett Field, California 2000.
- [3] Bousman, W. G., Kufeld, R. M., *UH-60A Airloads Catalog*, NASA/TM-2005-212827, 2005.
- [4] Bousman, W. G., *Rotorcraft Airloads Measurements-Extraordinary Costs, Extraordinary Benefits*, NASA/TP-2014-218374, Ames Research Center Moffett Field, California 2014.
- [5] Gula, P., Gorecki, T., *Design, Experiments and Development of a Polish Unmanned Helicopter ILX-27*, 39st European Rotorcraft Forum, Moscow 2013.
- [6] Johnson, W., *Milestones in Rotorcraft Aeromechanics*, NASA/TP-2011-215971, Ames Research Center Moffett Field, California 2011.
- [7] Johnson, W., *A History of Rotorcraft Comprehensive Analyses*, AHS 69th Annual Forum, Phonix, Arizona 2013.
- [8] Stalewski, W., *Aerodynamic designing and optimization of Rotorcrafts* (in Polish: Projektowanie i optymalizacja aerodynamiczna wiropłatów), Biblioteka naukowa nr 52, Wydawnictwo Naukowe Instytutu Lotnictwa, Warszawa 2017.
- [9] Wang, L., Diskin, B., Biedron, R. T., Neilsen, E. J., Sonnevile, V., Bauchau, O. A., *High-Fidelity Multidisciplinary Design Optimization Methodology with Application to Rotor Blades*, Aeromechanics Design for Transformative Vertical Flight, San Francisco, California 2018
- [10] Yeo, H., Romander, E. A., Norman, T. R., *Investigatioin of Rotor Performance and Loads of a UH-60A Individual Blade Control System*, Journal of the American Helicopter Society, Vol. 56, 2011.

Manuscript received 20 March 2019; approved for printing 28 June 2019